FIRE AND MATERIALS
*Fire Mater.* 2006; **30**:257–270
Published online 5 September 2005 in Wiley InterScience (www.interscience.wiley.com). DOI: 10.1002/fam.906

# A slug calorimeter for evaluating the thermal performance of fire resistive materials‡

D. P. Bentz[1,*,†], D. R. Flynn[2], J. H. Kim[3] and R. R. Zarr[1]

[1] *Building and Fire Research Laboratory, National Institute of Standards and Technology, Gaithersburg, MD 20899-8615, U.S.A.*
[2] *MetSys Corporation, Millwood VA 22646-0317, U.S.A.*
[3] *Photonics System Team, Korea Photonics Technology Inst., #459-3 Bonchon-Dong, Buk-Gu, Gwangju 500-210, Republic of Korea*

## SUMMARY

The utilization of a slug calorimeter to evaluate the thermal performance of fire resistive materials (FRMs) is presented. The basic specimen configuration consists of a 'sandwich', with a square central stainless-steel plate (slug) surrounded on two sides by the FRM. This sandwich configuration provides an adiabatic boundary condition at the central axis of the slug plate that greatly simplifies the analysis. The other four (thin) sides of the steel plate (and FRM specimens) are insulated using a low thermal conductivity fumed-silica board. Two metal plates manufactured from a high temperature alloy provide a frame for placing the entire sandwich specimen slightly in compression. The entire configuration is *centrally* placed at the bottom of an electrically heated box furnace and the temperatures of the metal slug and exterior FRM surfaces are monitored during multiple heating and cooling cycles. Knowing the heat capacities and densities of the steel slug and the FRM, an effective thermal conductivity for the FRM can be estimated. The effective thermal conductivity of the FRM will be influenced by its true thermal conductivity and by any endothermic or exothermic reactions or phase changes occurring within the FRM. Preliminary tests have been conducted on two commonly used FRMs and on a non-reactive fumed-silica board to demonstrate the feasibility of the method. Published in 2005 by John Wiley & Sons, Ltd.

KEY WORDS: fire resistive material; slug calorimeter; thermal conductivity

## INTRODUCTION

Fire resistive materials (FRMs) are currently generally evaluated using the ASTM standard test method E119 [1]. This test provides a time 'rating' for which the FRM will adequately protect a specific element or subsystem of a structure. Two of the major criteria determining the performance of a FRM are the measured average and maximum temperatures of a series of thermocouples placed on the (steel) substrate. While they are useful as practical failure criteria, these data alone provide little insight into the key thermal properties of the FRM that would allow a better understanding of its performance. The thermal performance of the FRM is

*Correspondence to: Dale Bentz, Building and Fire Research Laboratory, National Institute of Standards and Technology, Gaithersburg, MD 20899-8615, U.S.A.
† E-mail: dale.bentz@nist.gov


*Received 20 December 2004*
*Accepted 27 June 2005*
Published in 2005 by John Wiley & Sons, Ltd.

controlled by its heat capacity, density, thermal conductivity, and any heat released, absorbed, or transported due to chemical reactions (dehydrations, etc.) and phase changes [2]. The goal of this paper is to present an experimental set-up that maintains the 'spirit' of the ASTM E119 test set-up while providing detailed data on the fundamental thermophysical properties and thermal performance of the FRM.

The key components extracted from the ASTM E119 testing are that a steel substrate is protected by a specific thickness of FRM material and is exposed to a controlled temperature–time environment in a furnace. The test specimen size is reduced from the ASTM E119 testing to a square 152 mm × 152 mm specimen that is nominally 25 mm in thickness. Thermocouples are placed in the steel substrate and also at the 'exposed' surfaces of the FRMs to monitor dynamically the temperature gradient that exists across the sample. Additionally, by using a 'sandwich' specimen configuration and a central stainless steel plate of known mass and thermal properties, the heat flow through the FRM specimens can be easily estimated from a simple energy balance, taking advantage of the adiabatic boundary condition that exists at the central axis of the steel plate slug. Knowing the heat flow and the temperature gradient, an 'effective' thermal conductivity for the FRM as a function of temperature can be determined. This effective thermal conductivity will be influenced by the true thermal conductivity of the material, any endothermic or exothermic reactions occurring in the FRM, and any additional energy/mass transport due to vaporization of water (steam) and other reaction products formed from dehydration, decarbonation, etc. of the FRM material. The influence of these reactions can be conveniently explored by exposing the sandwich specimen to multiple heating/cooling cycles, as the reactions will likely be present only during the first heating cycle. This approach is presented in more detail in the sections that follow. A somewhat similar approach for determining an effective thermal conductivity of intumescent coatings using a cone calorimeter and numerical analysis has been presented recently [3].

## EXPERIMENTAL

### *Slug design*

An AISI Type 304 stainless steel plate 152 mm × 152 mm was cut from a sheet having a thickness of 12.7 mm. To monitor the temperature of the steel slug, three vertical holes 3.5 mm in diameter were milled into the plate along its central axis, extending 51, 76, and 102 mm into the plate's depth. The holes were located at distances of 51, 76, and 102 mm from the plate's edge. The steel plate mass was 2340 g. A density value of 8000 kg/m$^3$ for 304 stainless steel was taken from the literature [4], along with heat capacity values as a function of temperature [5], as shown in Figure 1. Before testing any FRM specimens, the steel plate was heated to a temperature of 973 K during two separate runs in the furnace. The plate can be optionally fitted with two allen screws (one on each side) to enable the final sandwich specimen to be suspended from an external balance on two wires. Care must be taken to assure that the wire diameter is sufficient to support the dead load during the temperature rise experienced during an actual test run. For our purposes, 16 gauge Chromel[§] wire has been found to be sufficient, while 24 gauge

[§] Certain commercial products are identified in this paper to specify the materials used and procedures employed. In no case does such an identification imply endorsement by the National Institute of Standards and Technology, nor does it indicate that the products are necessarily the best available for the purpose.

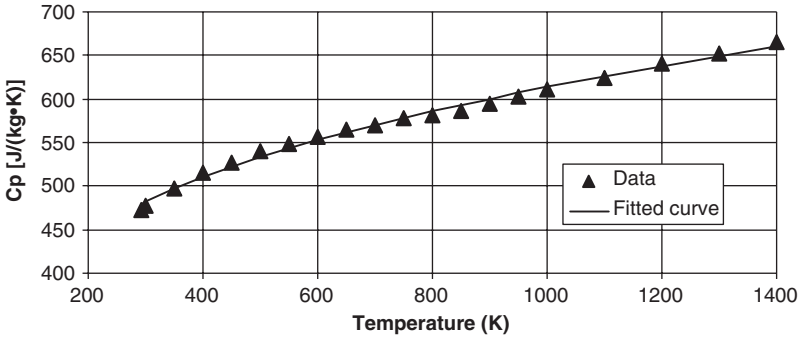


Figure 1. Literature values [5] and fitted curve for heat capacity of 304 stainless steel. Fitted curve is of the form $c_p = A + BT + C\ln(T)$ with $T$ in degrees K.

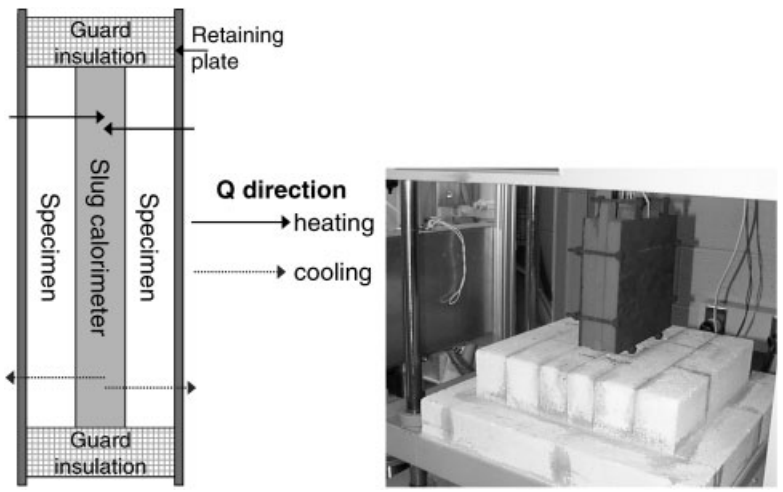


Figure 2. Schematic and photo of the slug calorimeter test set-up: left—schematic of a cross section through the middle of the basic slug calorimeter set-up, and right—photo of a completed sandwich specimen of the fumed-silica insulation board mounted and ready for testing in the furnace.

wire resulted in two premature failures during preliminary tests, with a total load on the order of 5000 g. Optionally, the final sandwich configuration can be set in the bottom centre of the (bottom loading) box furnace, as shown in Figure 2, if only temperatures and not mass are to be monitored during the test.

*Furnace setup*

All experiments were conducted in an electrically heated box furnace with a working volume of 360 mm × 360 mm × 360 mm and a maximum operating temperature of 1773 K. The bottom surface of the furnace is located on hydraulic elements and can be moved up and down

for loading and unloading of specimens (Figure 2). A series of five Type N thermocouples, insulated for high temperature applications, was introduced into the furnace through an entry port in the top. The thermocouples were connected to a constant temperature zone box, where their differential voltages were monitored using a digital multimeter and digital voltmeter. The thermocouples were monitored periodically and recorded on a computer. Measurement in ice water yielded an average standard deviation of 0.05 K among the five thermocouples.

*FRM and insulation material*

Samples of two mineral fibre/portland cement-based FRMs were obtained from a manufacturer. The samples were of nominal size 300 mm × 300 mm × 25 mm. Heat capacities, densities, and thermal conductivities of these materials had been previously determined by various laboratories [2,6,7]. Here, the two materials shall be designated as FRM A and FRM B. The room temperature densities of FRM A and FRM B were measured to be 314 kg/m$^3$ and 237 kg/m$^3$, respectively [6]. The heat capacity and mass loss measurements vs temperature for the two materials are provided in Figures 3 and 4. The testing laboratory reported their heat capacity values to be normally within $\pm$ 5% [6]. For each test run in the furnace, two panels of dimensions 152 mm × 152 mm × 25 mm were cut from the larger panels to use in the sandwich specimen configuration. The initial mass of each specimen was measured and recorded. The specimens of the FRMs were not pre-conditioned prior to evaluation in the box furnace.

A fumed-silica insulation board with a low thermal conductivity ($\approx$0.02 W/m K) was used both as thermal insulation in the sandwich configuration and as a non-reactive 'reference' material for evaluating the experimental set-up. The board is available as NIST Standard Reference Material 1449 (http://ts.nist.gov/) and its room temperature [8] and high temperature [9] thermal conductivities have both been previously measured by NIST. Specimens [8] were obtained in panels having nominal dimensions of 600 mm × 600 mm × 25 mm with a nominal bulk density of about 310 kg/m$^3$. For the purposes of this study, smaller sections were carefully

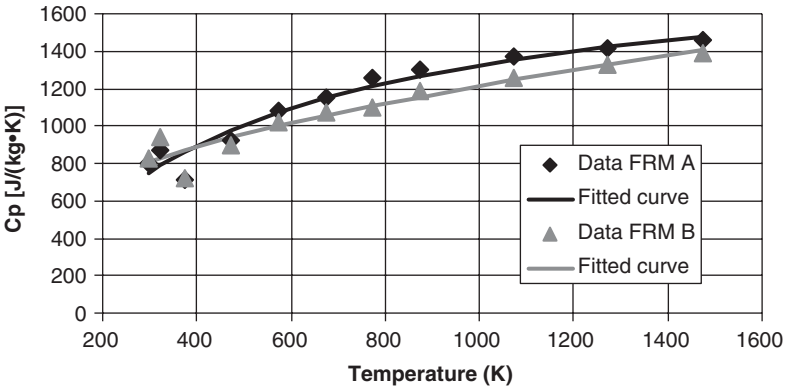


Figure 3. Measured values [6] and fitted curves for heat capacities vs temperature of the two FRMs. Fitted curves are of the form $c_p = A + BT + C\ln(T)$ with $T$ in degrees K.

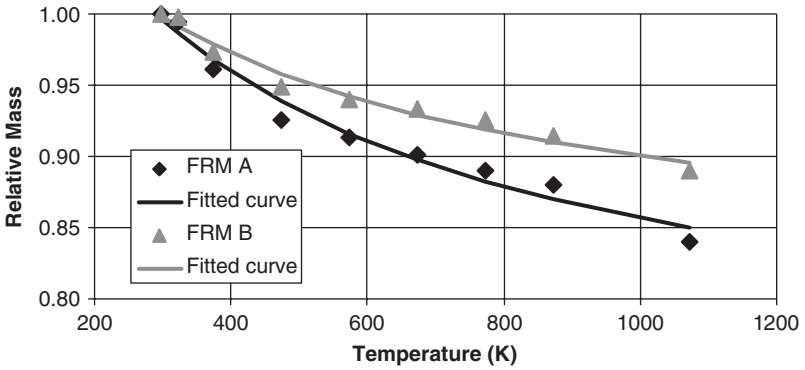


Figure 4. Values [6] measured according to ASTM E1131 [1] and fitted curves for mass loss vs temperature of the two FRMs. Fitted curves are of the form $M = A + BT + C\ln(T)$ with $T$ in degrees K.

cut as needed from one large panel using a hand saw. All samples were pre-conditioned overnight in a 373 K oven prior to being used as insulation or test specimens in the box furnace setup. The panels had been previously heat treated at 923 K for 8 h by the manufacturer [8]. The heat capacity of the fumed-silica board as a function of temperature was measured using a differential scanning calorimeter (DSC) and the ASTM E1269 standard technique [1] and determined to be in the order of (1000 $\pm$ 100) J/(kg K), in good agreement with the limited data available for similar materials currently in production.[¶]

*Testing procedure*

The specimens and slug plate were surrounded by a 63.5 mm (total thickness), 25.4 mm wide guard of the fumed-silica insulation board and mounted between two Inconel frame plates (see Figure 2). The entire assembly was held together by a set of eight retaining screws (two on each of the four edges of the plates). The assembled sandwich was either suspended from two wires or simply placed on the bottom centre of the box furnace and the thermocouples were mounted; three Type N thermocouples were placed at the various depths in the centre slug plate and one each was placed on the two exterior surfaces of the specimens being evaluated, between the specimens and the retaining Inconel plates. In addition to these thermocouples, the temperatures of the zone box and the furnace were also monitored and recorded. In most tests, the furnace temperature was programmed to follow a curve similar to the standard ASTM E119 temperature–time curve [1], but with a less rapid initial temperature rise, due to limitations on the heating rate of the furnace. The actual temperature–time curve employed will be shown in the results to follow. The tests were generally aborted by turning off the furnace power when the central steel slug reached an average temperature of 823 K, at which point the furnace itself had typically achieved a temperature in the range of 1173–1273 K. However, the thermocouples still monitored temperatures during cooling. Thus, while the heating portion of the tests generally occurred over a period of 1–2 h, the cooling portion could take as long as 24–48 h,

[¶] See for example: http://www.culimeta.de or http://www.microtherm.uk.com.

when the furnace was not opened to accelerate the cooling. Additional tests were conducted at slower heating rates to determine the sensitivity of the computed thermal conductivities to this parameter. Typically, the furnace temperature was linearly raised to 873 K during the course of either 4 or 16 h and then held there until the centre slug plate also attained nearly this temperature, at which point the furnace was turned off and a cooling curve monitored.

## ANALYSIS

Assuming one-dimensional heat flow through the FRM components of the specimen sandwich, a solution will be determined for the case where the temperature of the surfaces of the exposed specimens is increasing/decreasing at a constant rate. We consider a pair of FRM specimens, each of thickness $l$, with the initial condition that the temperature is constant through the thickness of the specimen and slug, i.e. $T(z,0)=0$. By symmetry, the mid-plane of the steel slug plate will be an adiabatic boundary, so that we need only consider one specimen and one half of the steel slug plate. Assuming constant properties, the temperature in the specimen must satisfy:

$$\frac{\partial^2 T}{\partial z^2}=\frac{1}{\alpha}\frac{\partial T}{\partial t} \tag{1}$$

where $\alpha=k/C$ is the thermal diffusivity ($m^2/s$), $k$ is the thermal conductivity ($W/(m\,K)$), $C=\rho c_p$ is the volumetric heat capacity ($J/(m^3\,K)$), and $\rho$ is density ($kg/m^3$), all for the FRM specimen material. The steel slug plate is assumed to have a sufficiently high thermal conductivity that it can be considered to be isothermal at any given time. The 'thermal capacity' of the slug plate, per unit area, is taken to be $2H=$ (areal density of the plate) $\times$ (heat capacity of the plate), with the factor of 2 arising from the fact that we need only consider one half of the steel slug plate. The thermal capacity, $H$, has units ($J/(m^2\,K)$).

The boundary condition at the exposed surface of the specimen, $z=0$, is

$$T(0,t)=Ft \tag{2}$$

where $F$ is the (constant) temperature increase rate having the units (K/s). The boundary condition at the specimen surface, $z=l$, which is in contact with the steel slug plate is

$$k\frac{\partial T}{\partial z}+H\frac{\partial T}{\partial t}=0 \tag{3}$$

which follows from the fact that the heat conducted out of this face of the specimen must equal the heat absorbed by (one half of) the steel slug plate.

Assuming that the transient (exponentially decaying) terms in the solution, which depend on the thermal diffusivity of the FRM specimen and time, can be neglected, we arrive at a solution of the form:

$$T(z,t)=F\left[t-\frac{(H+lC)z}{k}+\frac{Cz^2}{2k}\right] \tag{4}$$

The temperature difference across the specimen of the FRM, $\Delta T$, is

$$\Delta T=T(0,t)-T(l,t)=\frac{Fl}{k}\left[H+\frac{lC}{2}\right] \tag{5}$$

Finally, the thermal conductivity of the specimen can be computed as

$$k = \frac{Fl(H + (lC/2))}{\Delta T} \tag{6}$$

If the masses of the slug ($M_S$) and FRM specimen ($M_{FRM}$) are known, Equation (6) can be rewritten as

$$k = \frac{Fl(M_S c_p^S + M_{FRM} c_p^{FRM})}{2A\Delta T} \tag{7}$$

where $A$ is the cross-sectional area of the slug (or specimen, $0.152\,m \times 0.152\,m = 0.0232\,m^2$ in our experimental set-up), and $c_p^S$ and $c_p^{FRM}$ refer to the heat capacities of the steel plate and FRM specimen in units of (J/(kg K)), respectively. A similar analysis can be performed for the cooling case ($F<0$, $T(z,0) = \text{constant}$), and it can be shown that Equation (7) applies in this case as well.

Equation (7) was conveniently implemented in a spreadsheet programme to determine the effective thermal conductivity from the acquired temperature–time data points. The measured temperature-vs-time series for the slug and for the exterior FRM surfaces were used to compute the instantaneous values of $F$ ($\partial T/\partial t$ for the slug) and $\Delta T$ for use in Equation (7). Measured heat capacities of the 304 stainless steel (Figure 1) and FRMs (Figure 3) as a function of temperature and mass losses vs temperature for the FRMs (Figure 4) were used to further refine the parameters used in Equation (7). The resulting values of $k$ will be graphed against the mean FRM specimen temperature ($[T(0,t) + T(l,t)]/2$) in the results that follow. While this paper presents preliminary results to indicate the feasibility of utilizing the slug calorimeter method to evaluate the thermal performance and specifically the effective thermal conductivity of FRMs, an expanded uncertainty analysis could be conducted based on Equation (7) and the law of propagation of uncertainty [10]. Assuming that the heat capacities of the steel slug and the FRM specimen are fairly well known and that lengths and masses can be measured with less than 1% uncertainty, the uncertainties in the thermocouple measurements at high temperatures, which are used to calculate both $F$ and $\Delta T$ in Equation (7), will be the most significant contributors to the overall uncertainty. Thus, the uncertainty can be reduced simply by applying Equation (7) over a larger time interval. For example, assuming an optimistic uncertainty of 1 K for the thermocouple readings at high temperatures, changing the sampling frequency from 1 to 5 min reduces the estimated uncertainty in the effective thermal conductivity from about 25% to about 5% for thermal conductivities computed in the temperature range of 673–973 K during heating. During cooling, using a 25 min interval to calculate the effective thermal conductivity reduces its uncertainty to about 8% from a value of about 40% for 5 min intervals.

## RESULTS AND DISCUSSION

### *Fire resistive materials*

The thermocouple temperatures collected during a single heating/cooling cycle of FRM A are provided in Figure 5. The ASTM E119 standard temperature–time curve [1] is shown for comparison to the heating curve achievable in the electric furnace. It is worth noting that during a portion of the heating curve the mean exterior FRM surface temperature actually slightly exceeds the 'ambient' temperature of the furnace, most likely due to enhanced radiation transfer

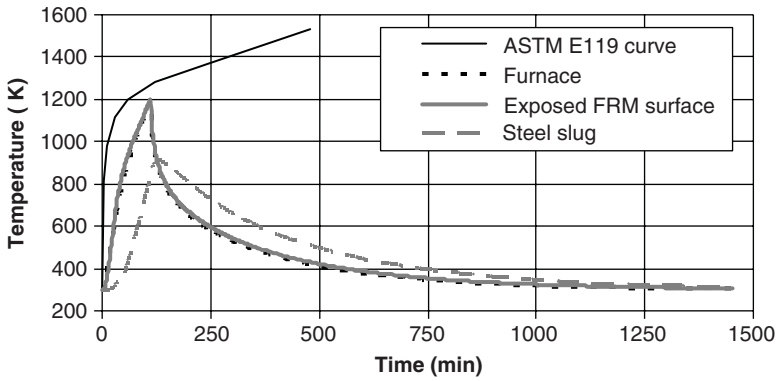


Figure 5. Measured temperature vs time data for one heating/cooling cycle for FRM A specimens.

between the Inconel retaining plates and the individual furnace heating elements. This reinforces the need to centre the sandwich specimen in the furnace, so that both sides (specimens) are exposed to nominally the same thermal environment. There was little variability observed among the three thermocouples mounted in the steel slug, indicating that the assumption that it behaves as an isothermal slug mass is a generally valid one. Since these three thermocouples are also mounted at different depths in the steel plate, a low variability among them also supports the validity of the assumption of one-dimensional heat transfer through the FRM that is critical to the quantitative analysis. In Figure 5, it is clearly observed that even after the furnace is turned off (as indicated by the peak in the furnace and outer FRM temperature curves near 100 min), the temperature in the steel slug continues to increase due to the thermal capacity (inertia) of the FRM specimens (and to some extent the retaining plates). When the interior temperature of the slug exceeds the exterior temperature of the FRM, the direction of the specimen heat flow reverses.

One performance criterion that could be conveniently extracted from the data in Figure 5 is the time necessary for the steel slug to reach some specific temperature, such as 811 K for example [1]. For the initial heating cycle of FRM A shown in Figure 5, approximately 105 min were required for the steel slug to achieve this temperature. For two subsequent heating cycles, these times were observed to be on the order of 110 min. These results suggest that most of the performance of this particular FRM is achieved via its 'low' thermal conductivity and not via the contribution of significant endothermic reactions, as will be discussed in more detail, when the computed thermal conductivity curves are presented below.

Equation (7) was applied to the data shown in Figure 5 and the computed thermal conductivity values for three different heating/cooling cycles are provided in Figure 6 in comparison to the previously measured values. One of the testing laboratories reported their results for thermal conductivity to be normally within $\pm$ 3% [6]. The first two heating cycles followed the furnace heating curve shown in Figure 5. A third heating cycle that also followed this same heating curve produced results (not shown for clarity) that were basically identical to those obtained in the second presented heating cycle. For the fourth heating cycle, as outlined above, the furnace temperature was linearly ramped to 873 K in 4 h. The cooling curve for the fourth cycle is incomplete due to a power outage that occurred during the course of that experimental run. Finally, a fifth heating cycle, in which the furnace temperature was linearly

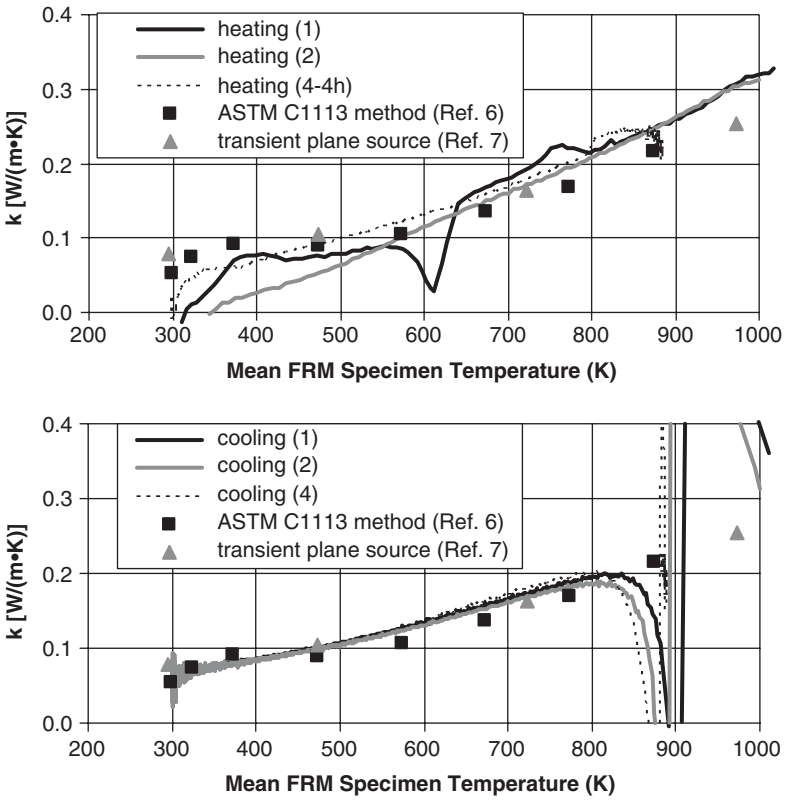


Figure 6. Effective thermal conductivity results for FRM A in comparison to measured data [6,7] for multiple heating (top) and cooling (bottom) cycles in the slug calorimeter.

ramped to 873 K in 16 h, produced results (not shown) quite similar to those generated in the fourth heating cycle.

The computed thermal conductivity values agree with the values measured previously using either a hot wire [6] (ASTM C1113 [1]) or a transient plane source method [7,11] to within 15% for temperatures up to 873 K. The computed values at temperatures above 873 K for the three presented heating cycles are clearly higher than those previously measured, which could possibly be due to enhanced heat transfer by radiation in these highly porous fibrous materials [12] sandwiched between the 'radiating' exterior Inconel plates and the interior steel slug. It is observed that, after the initial transients during which time the direction of heat flow is reversed and a new 'steady state' is established, the data for the three different presented cooling curves are all quite similar, indicating that equilibrium had been reached within the FRM with respect to reactions after the first heating cycle.

A comparison of the heating curves is even more informative. The differences among the heating curves for the first and the second runs should be indicative of the reactions, etc. occurring in the FRM. In the data in Figure 6, two phenomena appear to be contributing to these differences. First, there is an endothermic contribution, most likely due to dehydration of the hydrated cement component of the FRM. This is indicated by the downward 'peaks' in the

first heating curve that fall below the nominal thermal conductivity values. These endothermic reactions should reduce the heat flow through the specimen and thus appear as a reduction in the 'effective' thermal conductivity. In Figure 6, they are clearly present for mean FRM specimen temperatures between 573 and 673 K. Interestingly, prior to and beyond this range of temperatures, there appear to be several smaller exothermic peaks relative to the baseline curves. There are at least two possibilities for the cause of these apparent exotherms. One would be the presence of true exothermic reactions within the FRM, such as those that would be generally expected during the thermo-oxidative decomposition of any organic components within the material. The second (more likely) possibility is that this increase in effective thermal conductivity is due to the convection of superheated steam and gases created during the endothermic dehydration reactions. The particular FRMs evaluated in this preliminary study have a high porosity and a fairly open pore structure so that the steam produced during the dehydration reactions (and its accompanying energy) could be easily driven inward towards the stainless steel plate slug. This phenomenon would appear as an apparent increase in the effective thermal conductivity of the FRM material, and would likely only be present during the initial heating cycle. This same transport of steam/gas, or more specifically the lack thereof, is responsible for the often observed spalling of high-performance (low permeability) concrete during fire exposure [13].

In Figure 6, it can be observed that by combining the effective thermal conductivity results produced during a complete heating/cooling cycle such as cycle #2, a much larger temperature range can be covered than that covered by an individual heating or cooling curve. This is due to the transient effects present both during the initial part of the heating curve and during the transition that occurs as the direction of heat flow is reversed during the cooling cycle. Much of the transient effect on heating was removed when the heating rate was slowed to either $\approx$150 or $\approx$37.5 K/h, as illustrated by the 4 h results in Figure 6 for heating curve 4.

Based on these considerations, the following experimental procedure will be adopted for all future testing of FRMs using this slug calorimeter. The first two heating/cooling cycles will follow the heating curve shown in Figure 5, with natural cooling. Finally, a third heating/cooling cycle will consist of heating the furnace to 873 K slowly over the course of 4 h, then holding this temperature until it is also nearly achieved by the slug plate, followed once again by natural cooling. These three sets of curves will be used to characterize the thermal performance of the FRM as presented above.

The testing protocol outlined above was applied to the evaluation of FRM B. For the first two heating curves, times of 104 and 102 min, respectively, were required for the inner steel slug to reach a temperature of 811 K, slightly less than those observed for FRM A above. The effective thermal conductivities computed from Equation (7) are provided in Figure 7. The results are quite similar to those in Figure 6 with a few characteristic differences. In comparing the heating curves for the 1st and 2nd cycles in Figure 7, it is observed that the endotherms and exotherms are generally smaller in magnitude in comparison to those observed in Figure 6. This is consistent with the lower mass loss (less reaction) of FRM B relative to FRM A (Figure 4). In addition, there is some indication of an additional high temperature endothermic reaction present for FRM B, possibly due to decarbonation of the carbonated portland cement component of the FRM.

Secondly, there is a larger observed difference between the slug calorimeter and the previously measured thermal conductivities at higher temperatures ($>$673 K) than that observed in Figure 6. Because FRM B has a significantly lower density and higher (open) porosity than FRM A, it

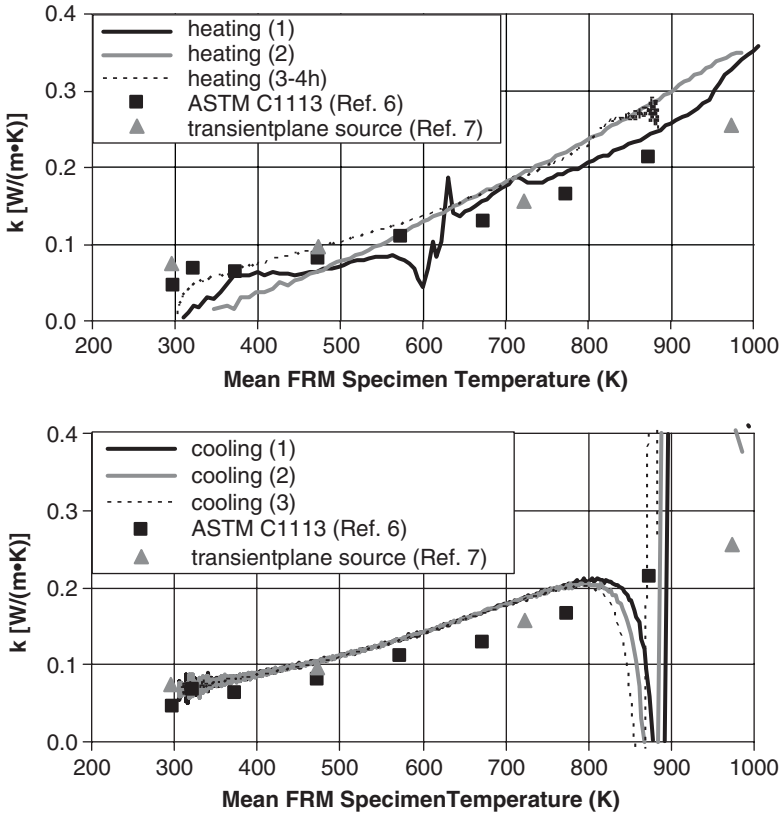


Figure 7. Effective thermal conductivity results for FRM B in comparison to measured data [6,7].

would be expected that any increased heat transfer due to radiation between the Inconel plates and the stainless steel slug would be enhanced in this material relative to FRM A. For temperatures below about 673 K, where these radiation effects would be expected to be much less significant, the agreement between the slug calorimeter effective thermal conductivity values and those previously measured is within 20%.

*Fumed-silica insulation board*

In addition to being used as a guard insulation material, the fumed-silica board was also utilized as the specimens themselves in one set of three heating/cooling cycles. The material contains no organic compounds and is non-reactive at temperatures up to 1173 K [8], so that the computed thermal conductivity results can be compared directly to the previously measured values [8,9]. However, an additional complication arises in this case. When the fumed-silica board is used only as guard insulation, it has a much lower thermal conductivity than the typical FRM specimens and the assumption of one-dimensional heat transfer through the thickness of the guarded square FRM specimens appears to be valid, as indicated by the results presented above. Conversely, when the fumed-silica board is used for the specimens

as well, the relative heat transfer through the 'guarded' areas of the sandwich configurations becomes significant. While the temperature rise of the slug is still indicative of the heat flow into the slug, the area ($A$ in Equation (7)) for this flow is no longer simply $0.152\,\text{m} \times 0.152\,\text{m}$. For the analysis presented below, it has been assumed that in this case, the total area available for heat transfer is given by the total area of specimen surrounded by the guard ($0.203\,\text{m} \times 0.203\,\text{m}$) plus the area of the thin sides of one half of the slug calorimeter (two times $0.203\,\text{m} \times 0.00635\,\text{m}$ plus two times $0.152\,\text{m} \times 0.00635\,\text{m}$). In addition, the mass of the 'FRM' specimen was taken as the mass of the fumed-silica insulation board specimen plus the masses of all of the guard materials comprising one half of the sandwich specimen configuration.

Physically, these first-order approximations seem reasonable and as shown in Figure 8, they do produce thermal conductivities for the cooling curves that are both reproducible and that

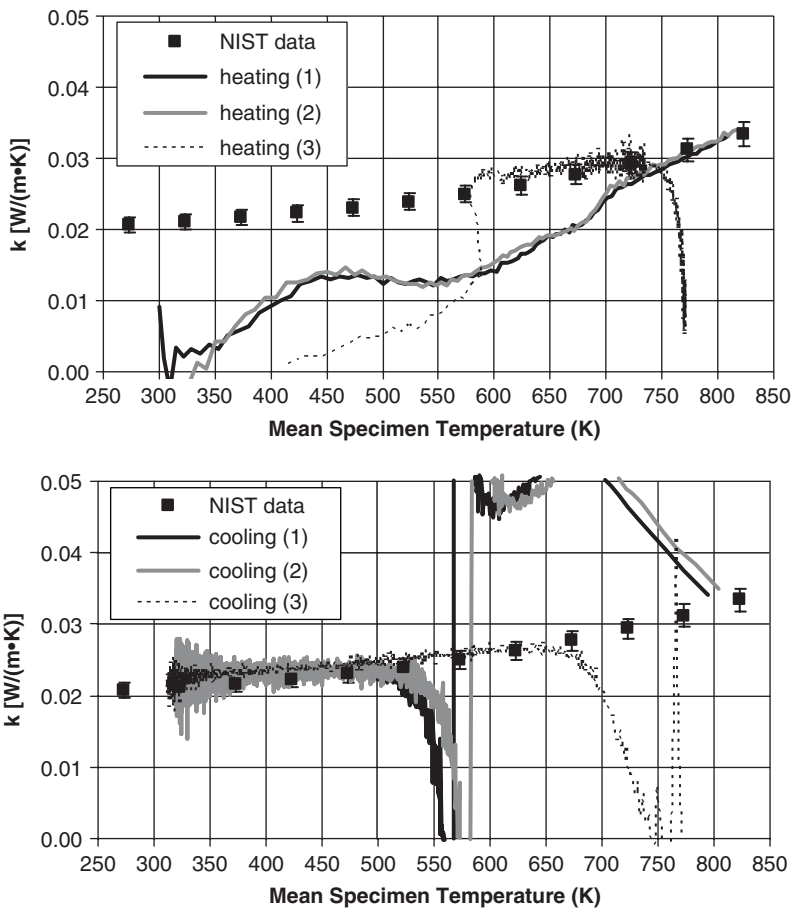


Figure 8. Computed effective thermal conductivity results for fumed-silica insulation board in comparison to previously measured NIST data (with error bars indicating $\pm$ 5%) [8,9]. Note: NIST data have been corrected to values for one standard atmosphere of pressure (sea level) using the procedure provided in Reference [9].

agree with the previously measured data to within about 5%. The data in Figure 8 appear much noisier than those in Figures 6 and 7, but it must be kept in mind that the scale on the $y$-axis in Figure 8 has been reduced by a factor of eight relative to that employed in the other two figures. One other point worth noting from Figure 8 is that once again, only the heating results for the third run, where a more gradual heating curve (extending only up to 773 K in this case) was employed, compare at all favourably to the gradual cooling results for the three runs and the previously measured data. In the first two runs that employed basically the same heating rate as that shown in Figure 5, due to the low thermal conductivity (and thermal diffusivity) of the fumed-silica board, 'steady-state' conditions were apparently only approached at the very end of the heating curve (773 K and beyond). The exponentially decaying terms neglected in arriving at Equation (4) above all involve an $\exp(-Xt)$ term where $X$ is linearly proportional to $k$. Thus, as $k$ decreases, a proportionally longer time $t$ will be necessary for these terms to become negligible. While it is beyond the scope of this initial feasibility study, the full solution to Equations (1)–(3) could be solved numerically to extract a better estimate of $k$ as a function of temperature during the heating tests of very low thermal conductivity materials.

The reproducibility of the heating and cooling curves for the first two runs in Figure 8 does provide further support that the fumed-silica board is indeed behaving as a non-reactive material over the temperature range employed in this preliminary study. The results for run 3 with the slower heating rate indicate once again the potential for piecing together the thermal conductivity values determined from the heating and cooling curves to provide a single thermal conductivity vs temperature curve that covers a larger temperature range than either of its two component curves. Radiation effects are seen to be of much less importance in this material as the computed values of $k$ agree well with those previously measured over the entire temperature range investigated with the slug calorimeter. Of course, the fumed-silica insulation board had been formulated specifically to minimize radiation transfer at high temperatures via the addition of an opacifier [8].

The first two heating tests with the fumed-silica insulation board were terminated when the *exterior* of the specimens reached a temperature of about 1173 K, quite similar to the termination point used for the testing of the two FRMs. However, in comparison to the FRMs, where the slug had achieved a temperature of about 810 K at this point, for the fumed-silica board, the interior slug temperature was still *well below* 470 K at this time. Naturally, this reinforces the critical importance of using a low thermal conductivity material to protect steel structures exposed to fire.

## CONCLUSIONS AND FUTURE DIRECTIONS

The use of a slug calorimeter for evaluating the thermal performance of fire resistive materials has been successfully demonstrated. Key components of the system include the use of a 'sandwich' specimen to provide an adiabatic boundary condition at its central axis and the utilization of multiple heating/cooling cycles to provide information on the influence of reactions and convective transport on the computed effective thermal conductivity values. The results obtained in this relatively simple small scale test can provide valuable insights into the mechanisms through which the FRM protects the steel substrate in an actual fire.

The experimental set-up presented in this paper has recently been modified to include an exhaust fume hood at the top of the furnace so that it may be applied to a wider variety of FRMs that emit organics as well as water and $CO_2$. Additionally, a set of retaining plates with a central 152 mm × 152 mm square hole has been produced, so that intumescent coatings that undergo considerable expansion during high temperature exposure have also been recently successfully evaluated using the slug calorimeter experimental set-up.

## REFERENCES

1. ASTM. *ASTM Annual Book of Standards*. ASTM International: West Conshohocken, 2004.
2. Bentz DP, Prasad KR, Yang JC. Towards a methodology for the characterization of fire resistive materials with respect to thermal performance models. *Fire and Materials* (in press).
3. Bartholmai M, Schriever R, Schartel B. *Fire and Materials* 2003; **27**:151.
4. ASM International. *Metals Handbook* (10th edn). ASM International: Materials Park, 1990.
5. Bogaard RH, Desai PD, Li HH, Ho CY. *Thermochimica Acta* 1993; **218**:373.
6. Anter Laboratories, Inc. Transmittal of test results, *Report to NIST*, 2004.
7. Dinges C (Hot Disk Laboratories). Report on measurements on samples supplied by NIST. *Report to NIST*, 2004.
8. Zarr RR, Somers TA, Ebberts DF. Room-temperature thermal conductivity of fumed-silica insulation for a standard reference material. *NISTIR 88-3847*. U.S. Department of Commerce, October 1988.
9. Smith DR, Hust JG. Microporous fumed-silica insulation board as a candidate standard reference material of thermal resistance. *NISTIR 88-3901*. U.S. Department of Commerce, October 1988.
10. Taylor BN, Kuyatt CE. Guidelines for evaluating and expressing the uncertainty of NIST measurement results. *NIST Technical Note No. 1297*. U.S. Department of Commerce, Washington, D.C., September 1994.
11. Gustafsson SE. *Review of Scientific Instruments* 1991; **62**(3):797.
12. Flynn DR, Gorthala R. Radiation scattering versus radiation absorption—effects on performance of thermal insulation under non-steady-state conditions. *Insulation Materials*: *Testing and Applications*: *Third Volume*, *ASTM STP 1320*. ASTM: West Conshohocken, 1997; 366.
13. Bentz DP. *ACI Materials Journal* 2000; **97**(3):351.